Mohamed, A., Ardyani, T., Bakar, S. A., Sagisaka, M., Umetsu, Y., Hussin, M. R. M., Ahmad, M. K., Mamat, M. H., King, S., Czajka, A., Hill, C., & Eastoe, J. (2018). Preparation of conductive cellulose paper through electrochemical exfoliation of graphite: The role of anionic surfactant ionic liquids as exfoliating and stabilizing agents. *Carbohydrate Polymers*, *201*, 48-59. https://doi.org/10.1016/j.carbpol.2018.08.040

Preparation of conductive cellulose paper through electrochemical exfoliation of graphite: The role of anionic surfactant ionic liquids as exfoliating and stabilizing agents

Azmi Mohamed[1,2*], Tretya Ardyani[1], Suriani Abu Bakar[2], Masanobu Sagisaka[3], Yasushi Umetsu[3], Mohd Rofei Mat Hussin[4], Mohd Khairul Ahmad[5], Mohamad Hafiz Mamat[6], Stephen King[7], Adam Czajka[8], Christopher Hill[8], Julian Eastoe[8]

[1]Department of Chemistry, [2]Nanotechnology Research Centre, Faculty of Science and Mathematics, Universiti Pendidikan Sultan Idris, 35900 Tanjong Malim, Perak, Malaysia

[3]Department of Frontier Materials Chemistry, Graduate School of Science and Technology, Hirosaki University, Bunkyo-cho 3, Hirosaki, Aomori 036-8561, Japan

[4]MIMOS Semiconductor Sdn Bhd (MSSB), Technology Park Malaysia, 57000 Bukit Jalil, Kuala Lumpur

[5]Microelectronic and Nanotechnology – Shamsuddin Research Centre (MiNT-SRC), Faculty of Electrical and Electronic Engineering, Universiti Tun Hussein Onn Malaysia, 86400 Parit Raja, Batu Pahat, Johor, Malaysia

[6]NANO-SciTech Centre (NST), Institute of Science (IOS), Universiti Teknologi MARA (UiTM), 40450 Shah Alam, Selangor, Malaysia

[7]Rutherford Appleton Laboratory, ISIS Spallation Source, Chilton, Oxfordshire, OX110QT, United Kingdom

[8]School of Chemistry, University of Bristol, Cantock's Close, Bristol, BS8 1TS, United Kingdom

*Corresponding author. Tel.: +601548797582; fax: +601548797296

E-mail address: azmi.mohamed@fsmt.upsi.edu.my

Abstract

A facile electrochemical exfoliation method was established to efficiently prepare conductive paper containing reduced graphene oxide (RGO) with the help of single chain anionic surfactant ionic liquids (SAILs). The surfactant ionic liquids are synthesized from conventional organic surfactant anions and a 1-butyl-3-methyl-imidazolium cation. For the first time the combination of SAILs and cellulose was used to directly exfoliate graphite. The ionic liquid 1-butyl-3-methyl-imidazolium dodecylbenzenesulfonate (BMIM-DBS**)** was shown to have notable affinity for graphene, demonstrating improved electrical properties of the conductive cellulose paper. The presence of BMIM-DBS in the system promotes five orders of magnitude enhancement of the paper electrical conductivity (2.71×10^{-5} S cm^{-1}) compared to the native cellulose (1.97×10^{-10} S cm^{-1}). A thorough investigation using electron microscopy and Raman spectroscopy highlights the presence of uniform graphene incorporated inside the matrices. Studies into aqueous aggregation behaviour using small-angle neutron scattering (SANS) point to the ability of this compound to act as a bridge between graphene and cellulose, and is responsible for the enhanced exfoliation level and stabilization of the resulting dispersion. The simple and feasible process for producing conductive paper described here is attractive for the possibility of scaling-up this technique for mass production of conductive composites containing graphene or other layered materials.

Keywords: surfactant, ionic liquids, reduced graphene oxide, self-assembly, electrochemical exfoliation, surfactant ionic liquids

Nomenclature

CVD	:	Chemical vapor deposition
GCP	:	graphene/cellulose paper
GO	:	Graphene oxide
ILs	:	Ionic liquids
NRL	:	Natural rubber latex
RGO	:	Reduced graphene oxide
SAILs	:	Surfactant ionic liquids
SANS	:	Small-angle neutron scattering
SDBS	:	Sodium dodecylbenzenesulfonate
SDS	:	Sodium dodecylsulfate
SLD	:	Scattering length density
VOCs	:	Volatile organic compounds
$I(Q)$	:	Scattering intensity
I_D/I_G	:	The ratio between the intensity of D- and G-band
$P(Q)$	:	Scattering form factor
R_a	:	Polar axis ratio of ellipsoidal micelle
$R_{cylinder}$	:	Cylindrical micelle radius
R_{disk}	:	Stacked disk radius
R_{sphere}	:	Spherical micelle radius
$S(Q)$	:	Structure factor (interparticle interaction)
X	:	Aspect ratio of ellipsoidal micelle
ζ-potential	:	Zeta potential
σ	:	Electrical conductivity

1. Introduction

Growing global concerns over the environment and sustainability are directing the development of next generation renewable materials. Biomaterials or biocomposites are considered as promising materials over synthetic polymers and can be used in industrial or smaller scale process. With the annual production estimated over 7.5×10^{10} ton per year (Pinkert, Marsh, Pang, & Staiger, 2009), cellulose is hailed as the most abundant renewable material in the world. Cellulose is often extracted from plant cells i.e. wood pulp and can find immediate use in the paper industry or other specific applications. It has several attractive properties including biodegradability, biocompatibility, and superior chemical stability, consequently represents as the most promising resource for producing biocomposites (Abdul Khalil, Ireana Yusra, Bhat, & Jawaid, 2010; Abdul Khalil, Bhat, & Ireana Yusra, 2012).

Introduction of electric fillers into a cellulose paper can switch the electrical properties of the resulting paper and make it possible for applications in flexible energy storage devices, electrodes, and sensors (Kang, Li, Hou, Wen, & Su, 2012; Kiziltas et al., 2016; Weng et al., 2011; Ye et al., 2016; Yoon, Jin, Kook, & Pyun, 2006). There is an ever-increasing interest in the utilization of graphene (and its derivatives) as a reinforcing filler in nanocomposites, and its attractive properties make it particularly suitable for the development of novel electrical cellulose paper. However, both cellulose and graphene present problems regarding dispersibility/solubility in aqueous solution (Hernandez, Lotya, Rickard, Bergin, & Coleman, 2009; Lindman, Karlström, & Stigsson, 2010; Medronho, Romano, Miguel, Stigsson, & Lindman, 2012). Without modifications to the chemical structure or the use of dispersing agents, it is rather challenging to obtain a good dispersion of cellulose and graphene in water (Roy, Semsarilar, Guthrie, & Perrier, 2009).

Current pre-treatments of cellulose dissolution typically employ acids and bases, and sometimes involves cuprammonium and xanthate which use relatively harsh processing solvents (traditional dissolution) (Zhang et al., 2009; Zhou & Zhang, 2000; Zhu et al., 2006). Other efforts have used ionic liquids (ILs) to achieve dissolution/dispersion. Ionic liquids (ILs) are considered as environmentally benign solvents replacement for volatile organic compounds (VOCs) due to their low vapor pressures, inflammability and recyclability (Chiappe & Pieraccini, 2005; Earle & Seddon, 2000). Reports have shown that some hydrophilic ILs based on imidazolium are able to dissolve large amounts of cellulose. Readers may refer to the seminal paper of Pinkert and co-workers for reference (Pinkert et al., 2009). Along with this, a number of other works have pointed out that ILs are suitable solvents to produce stable graphene dispersions with high concentrations (Bari et al., 2014; Liu et al., 2008; Nuvoli et al., 2011).

Ionic liquids offer tuneability and there are a huge number possibilities to alter their properties by modifying chemical structure (Chiappe & Pieraccini, 2005). A notable advancement in the field of ILs is the discovery of anionic surfactant ionic liquids (SAILs) (Brown et al., 2011; Brown et al., 2012). These compounds may act as solvents with the ability to self-assemble, offering unique opportunities to solving problems between two incompatible materials. Without doubt, SAILs will be useful in tailoring the incompatibility between graphene and cellulose to fabricate electric cellulose paper. To the Authors' knowledge, such a system has not been tested either for graphene or nanocomposite processing.

Ever since graphene hit the headlines, there has been a large body of work devoted to its synthesis and properties. Sophisticated techniques such as chemical vapor deposition (CVD) or the tedious mechanical exfoliation do tend to produce high quality graphene films (Whitener Jr & Sheehan, 2014), however, these methods are not suitable for bulk material applications. A low-

cost process to make graphene by exfoliating graphite layers may result readily-dispersed graphene that can find applications in polymer composites, conductive inks, and supercapacitors. The process can be performed efficiently through electrochemical treatment in surfactant solutions that provides colloidal stability (Alanyalıoğlu, Segura, Oró-Solè, & Casañ-Pastor, 2012; Kakaei & Hasanpour, 2014; Suriani et al., 2016). Interest in this technique stems from the simple experimental setup: graphite rods as working electrodes, immersed in a surfactant solution as the electrolyte, and a DC power supply. Although many studies on electrochemical exfoliation of graphite in surfactant solution are successful, they all focus on exfoliation effectiveness, and graphene or composite characteristics. Unfortunately, the surfactant aspect is relegated to just a stabilizing agent.

This present work reports simple and facile fabrication of nanofibrillated cellulose paper from kenaf (*Hibiscus cannabinus L.*) by directly exfoliating graphene in cellulose/SAILs dispersions, which is then followed by reduction of the suspension to obtain graphene/cellulose paper (GCP). Kenaf is well known as a cellulosic source with both economic and ecological advantages. After a decrease of the woods sources for pulp processing, one of the most sought out materials for papermaking is from kenaf (*Hibiscus cannabicus* L.) tree. Aside from the feasibility to be processed into pulps, it can be used as building materials or bio composites. It has many advantages to name as being inexpensive and requires minimal care since it can grow in a wide range of climatic conditions. Given this conditon, it is such an advantage to explore the most promising application of kenaf-based materials for improved value (Abdul Khalil, Ireana Yusra, Bhat, & Jawaid, 2010; Abdul Khalil, Bhat, & Ireana Yusra, 2012).

This paper aims to investigate the effect of modifying the counterion of conventional surfactants, thus turning them into SAILs, towards their ability in stabilizing aqueous systems

consisting of graphene and cellulose fiber. The SAILs are designed by exchanging a conventional sodium counterion of commercial surfactants sodium dodecylsulfate (SDS) and sodium dodecylbenzenesulfonate (SDBS) with a large organic 1-butyl-3-methyl imidazolium (BMIM) cation. The structures of the surfactants and SAILs are given in Table 1. Here, the surfactant and SAILs performances are studied in terms of the GCP electrical conductivity. The results showed that the applied strategy gives a subtle effect on the ability of the SAILs to stabilize the aforementioned system over their conventional surfactants. Significantly, this study provides new alternatives for generating environmentally friendly and economic graphene-compatible compounds considering that the starting materials are cheap and the synthesis process is simple.

2. Materials and methods

2.1 Materials

Sodium dodecylsulfate (SDS) and sodium dodecylbenzenesulfonate (SDBS) was purchased from Sigma Aldrich without further purification. 1-butyl-3-methyl-imidazolium chloride (99%) was obtained from Merck and used as received. Nanofibrillated kenaf cellulose was supported by Forest Research Institute Malaysia.

2.2 SAILs synthesis

The SAILs were synthesized and purified following on previous work by Brown et al.(Brown et al., 2012) The synthesized SAILs were characterized by ^{1}H NMR spectroscopy; all are consistent with the expected values (see **Supplementary Material**).

2.3 Graphene/Cellulose Paper (GCP) Preparation

Nanofibrillated kenaf cellulose (2.5 g) was first dispersed in surfactant/SAILs solution (50 mL) for 2 hours under vigorous stirring until forming stable dispersion. High purity graphite rods with a diameter of 10 mm and 150 mm in length were used as the electrodes. The as-prepared cellulose/SAILs (or surfactant) mixture was then used as electrolyte for the exfoliation process at a constant voltage of 7V (GW INSTEK GPS 303000). The electrochemical exfoliation was carried out under room temperature for 24 hours. The obtained dispersion was then subjected to mechanical stirring and sonication for 1 hour to form a homogeneous mixture of graphene oxide (GO)/cellulose/stabilizer. To the resulting mixture, a suitable amount of hydrazine hydrate (0.1 mL hydrazine /10 mL GO dispersion) was added and the reaction carried out under reflux condition at 90 – 100 °C for 24 hours to. After the reaction was considered complete, the mixture was then moved to a filter paper and left to dry overnight in an oven at 50 °C. A dark grey composite paper containing reduced graphene oxide (RGO) henceforth labelled as GCP obtained by peeling the paper from filter paper. The route to prepare GCP is sumarized in Fig. 1. Details on the amount of materials used for the preparation of GCP can be found in supplementary material Table S2.

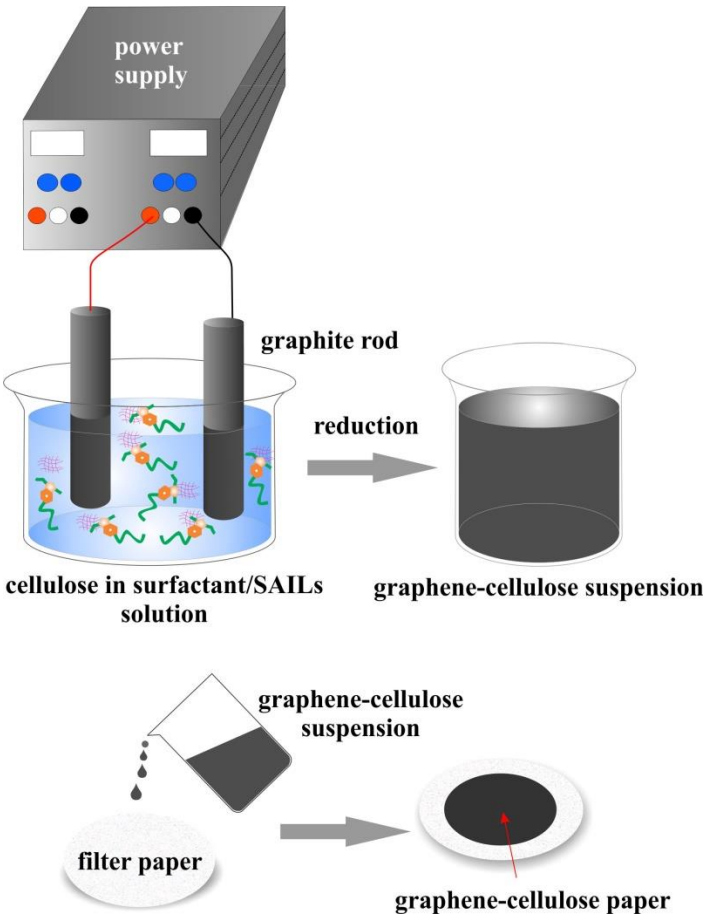

Fig. 1. Schematic of the GCP preparation

2.4 GCP Characterization

The electrical conductivity of GCP with dimensions of 15 x 15 mm and thickness ~ 0.10 mm was measured by a four-point probe method (Keithley 2636A). The measurement was repeated 5 times to ensure accuracy. The morphologies and microstructure of GCP were observed under field emission electron microscope (FESEM, Hitachi SU8020). Raman spectroscopy was carried out using a Renishaw InVia micro Raman system spectrofotometer with a 514 nm argon-ion laser source. Five regions were measured for each paper. To visualize the embedded microstructure of

cellulose paper using HRTEM (JEOL 2100F), the samples were ultramicrotomed with a diamond knife to give sections with nominal thickness ~80 nm.

2.5 Zeta potential measurements

Zeta potential measurements were performed by ELSZ-1000 Zeta-potential and Particle Size Analyzer (Photal OTSUKA ELECTRONICS) with Smoluchowski equation as zeta potential conversion equation and 1 peak Lorentz fitting. Measurements were carried out with a flow cell at sampling time 400 μs, cumulative number 7, measuring angle 15º, temperature 25 ºC, pin hole size 50 μm, cell constant 70.000 cm^{-1}. Properties of aqueous mixtures (refractive index 1.3328, viscosity 0.8878 cP, and permittivity 78.3 Fm^{-1}) were used for calculation of zeta potential. Zeta potential values were finally obtained as average values of 10 runs for each sample.

2.6 Small-angle neutron scattering (SANS)

Small-angle neutron scattering (SANS) studies were carried out on the time-of-flight LOQ instrument at ISIS, UK. The accessible *Q* range was 0.007 – 0.23 $Å^{-1}$, arising from incident neutron wavelengths of λ = 2.2 – 10 Å. Absolute intensities for *I(Q)* (cm^{-1}) were determined to within 5% by measuring the scattering from a partially deuterated polymer standard. Neutrons are scattered by short-range interactions with sample nuclei, the 'scattering power' of different components being defined by a scattering-length density (SLD), ρ (cm^{-2}). The samples were prepared in 2 mm path-length quartz cells and held on a thermostatted automatic sample changer at 25°C. Data have been fitted using the SASView interactive fitting program, fixing scattering length density differences as calculated and fitting for micellar volume fraction and appropriate structural

parameters as required by the different scattering laws. Scattering length density of surfactants, SAILs and graphene are given in **Supplementary material**.

Table 1

Surfactants and SAILs used in this study

Name	Chemical Structure and Name
SDS	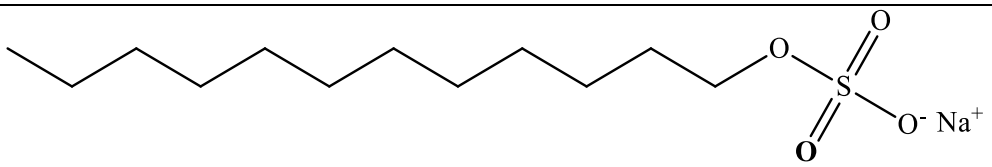 Sodium dodecylsulfate
SDBS	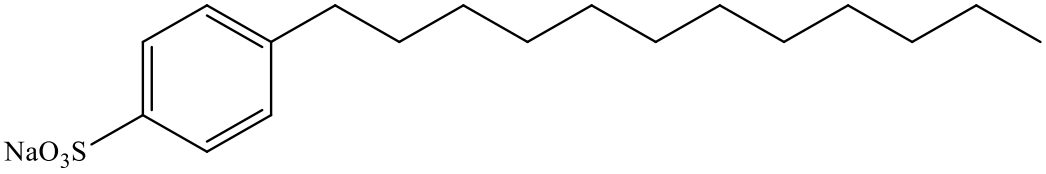 Sodium dodecylbenzenesulfonate
BMIM-DS	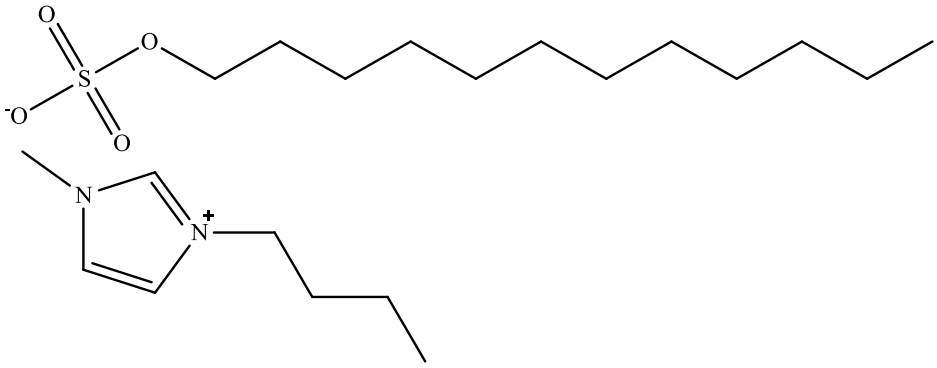 1-butyl-3-methyl-imidazolium dodecylsulfate

BMIM-DBS

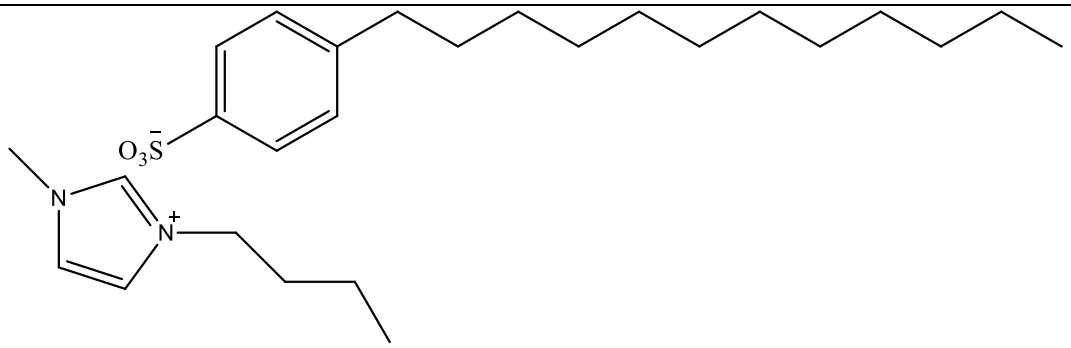

1-butyl-3-methyl-imidazolium dodecylbenzenesulfonate

3. Results and discussion

3.1 Electrical conductivities of graphene/cellulose paper (GCP)

To obtain an ideal conductive network, it is required that the graphene nanofillers be well separated despite the ever present van der Waals forces, and that a high dispersity of the nanofiller be maintained in the resulting cellulose nanocomposite. Poor dispersion of reinforcing nanostructures at the nanoscale, and weak interfacial interactions, may result in composites with limited enhancement in electrical conductivity. In an attempt to meet these requirements, many researchers have tried to develop conductive composites with various fabrication methods. Being electrically non-conductive in nature, here nanofibrillated kenaf cellulose (1.97×10^{-10} S cm^{-1}) was converted to an electrically conductive nanocomposite by incorporation of reduced graphene oxide (RGO) stabilizer surfactant and SAILs.

Uniform dark grey composite papers were obtained as thin discs with a diameter of 7.00 cm and 0.15 – 0.19 mm thickness. To evaluate the efficiency of surfactants in exfoliating graphite and stabilizing the graphene/cellulose dispersion system, a series of surfactant concentrations were used ranging from 0.05 M to 0.1 M. The GCP electrical conductivities as a function of surfactant concentration are summarized in Table 2 and Fig. 2. It is important to note that the electrical

measurements reported herein are for one-sided samples, however, both surface produce identical results due to good dispersion.

Clearly, replacement of the sodium counterions (Na^+) with imidazolium cations subtly changes the ability of the SAILs in stabilizing system comprising of RGO and cellulose. GCPs prepared with SAILs have electrical conductivities (σ) a little higher (~ 1 order of magnitude) than if prepared with its sodium analogue (see Table 2). The optimum electrical conductivity enhancement, attaining five orders of magnitude enhancement, was obtained by 0.1 M BMIM-DBS (2.71×10^{-5} S cm^{-1}). The effectiveness of these ionic liquids and cellulose combinations for direct exfoliation of graphite is very interesting. A similar concept, but using tip sonication, was recently reported (Ye et al., 2016). Although the electrical properties were studied in terms of charge-discharge capacities (and cannot be used as a direct comparison for this study), the resulting composites exhibited attractive potential for application as anode materials. A previous study utilizing regenerated cellulose with DMAC/LiCl reported an electrical conductivity of 3.7×10^{-6} S cm^{-1} while another using NaOH as a processing aid yielded a cellulose composite with 1.1×10^{-6} S cm^{-1} (Feng, Zhang, Shen, Yoshino, & Feng, 2012; Zhang, Liu, Zheng, & Zhu, 2012). It is therefore important to mention that the fabrication approach here is a facile, fast, inexpensive and versatile process to constructing materials from various complementary materials.

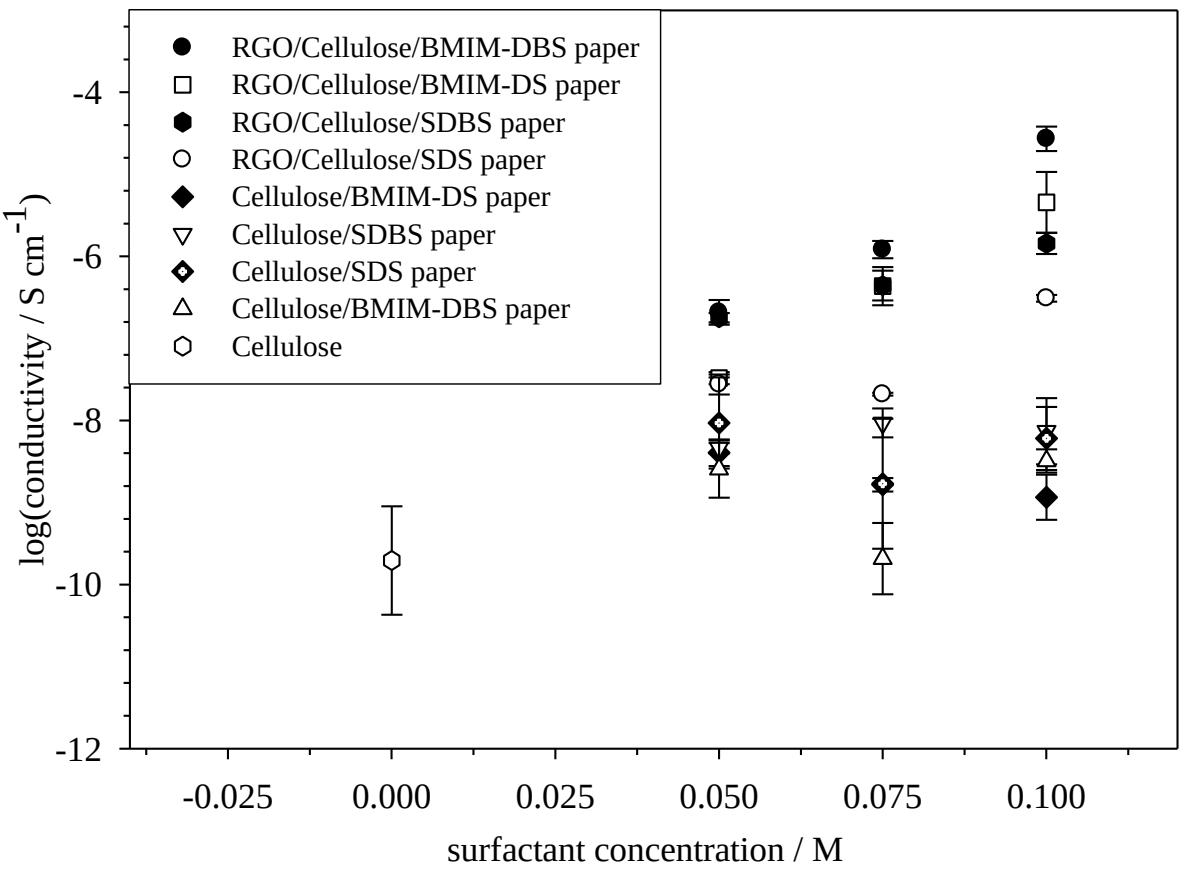

Fig. 2. Electrical conductivities of the nanofibrillated kenaf cellulose paper, nanofibrillated kenaf cellulose with surfactant/SAILs paper and GCP containing surfactants and SAILs. The error bars are given for five experimental measurements.

This increased electrical properties observed here may be influenced by the good combination of cellulose/ionic liquid as graphite exfoliant and dispersion stability. Due to its insolublity in water (pH 7) and recalcitrance to dissolve in organic solvents, cellulose has often been viewed as a hydrophobic material (Lindman et al., 2010; Medronho & Lindman, 2014; Medronho & Lindman, 2015). Recently, however, it is suggested that cellulose may display amphiphilic properties that can affect its dissolution/dispersion (Lindman et al., 2010; Medronho & Lindman, 2015). The hydrogen bonding of the heterocyclic ring BMIM counterions which is

assumed to compensate for the hydrophilic character probably plays an important role for the interaction with the hydrophilic parts of cellulose (Brown et al., 2012).

From a general viewpoint, gradually increasing the concentration of surfactant led to modest increases in the electrical conductivities. Again reiterating the importance of surfactant concentration in exfoliation and keeping the exfoliated layer stably dispersed (Lotya et al., 2009; Mohamed et al., 2018; Suriani, Nurhafizah, Mohamed, Zainol, & Masrom, 2015; Wang, Yi, & Shen, 2016). It was hypothesized that the chosen surfactant concentrations (0.05 – 0.1 M) are sufficient to form a network that provides electrical pathways, considering the significant σ from neat cellulose, and that the presence of RGO enveloping the cellulose network did assist the development of the electrical conductivity of the paper. This observation agrees with previous research on graphene/natural rubber latex (NRL) composites, showing surfactant at a concentration of 0.1 M produces composites with the highest electrical conductivity (Suriani et al., 2016; Suriani et al., 2015). It is instructive to compare these σ values with those systems without surfactants or SAILs. An attempt was made to exfoliate graphite using cellulose dispersion without surfactant or SAILs, however it was unsuccessful, and the resulting nanocomposite electrical conductivity could not be determined using four point probe measurement. As shown in Table 2 the presence of surfactant alone does not significantly affect the cellulose paper electrical conductivity. Clearly, the enhancement of electrical properties of cellulose papers are due to the RGO dispersed in the system.

Table 2

Electrical conductivities of nanofibrillated kenaf cellulose paper with and without RGO and the zeta (ζ)-potential values of RGO dispersion stabilized by surfactants and SAILs

Surfactant	Zeta (ζ)-potential of RGO dispersion (mV)	Surfactant concentration (M)		
		Electrical conductivity (S cm^{-1})		
		0.050	0.075	0.100
With RGO				
SDS	-43 ± 4	2.82×10^{-8}	2.08×10^{-8}	3.09×10^{-7}
SDBS	-40 ± 8	1.80×10^{-7}	4.67×10^{-7}	1.48×10^{-6}
BMIM-DS	-36 ± 1	3.30×10^{-8}	4.74×10^{-7}	5.86×10^{-6}
BMIM-DBS	-59 ± 1	2.17×10^{-7}	1.23×10^{-6}	2.71×10^{-5}
Without RGO				
SDS	-	6.03×10^{-9}	5.76×10^{-9}	9.32×10^{-9}
SDBS	-	5.73×10^{-9}	9.32×10^{-9}	4.59×10^{-9}
BMIM-DS	-	1.37×10^{-9}	1.64×10^{-9}	4.04×10^{-9}
BMIM-DBS	-	3.34×10^{-9}	4.38×10^{-10}	2.55×10^{-9}

3.2 Raman spectroscopy

Carbon allotropes show their fingerprints under Raman spectroscopy mostly by D, G, and 2D bands that lie around 1350, 1580, and 2700 cm^{-1}, respectively (Dresselhaus, Jorio, Hofmann, Dresselhaus, & Saito, 2010; Ferrari et al., 2006). Identification of these features allows characterization of graphene layers in terms of number of layers present or presence of defects can be observed in either GO and RGO (Ferrari et al., 2006). The band near 1580 cm^{-1} arises due to the in plane vibration of the sp^2 hybridization of carbon atoms. Meanwhile, the D band appears

due to the presence of disorder in atomic arrangement or edge effect of graphene, ripples, and charge puddles (Dresselhaus et al., 2010). The ratio between the intensity of D- and G-band (I_D/I_G) has been widely used an indicator of the amount of disorder in RGO sheets. Comparison of Raman spectra between the GCPs and graphite is shown in Fig 3.

The Raman spectrum of the pristine graphite is expected display a prominent G peak at 1581 cm^{-1} and a very low intensity of D peak at 1354 cm^{-1} hence the I_D/I_G value of 0.03. The Raman spectrum of the GCPs also contains a G band that is now broadened and shifted to around 1585 – 1594 cm^{-1}. In addition, the D band at 1347 – 1350 cm^{-1} becomes more prominent therefore giving an increased D/G intensity ratio compared to that in graphite. These alterations suggest changes in sp^2 domains upon reduction of the resulting GO through electrochemical exfoliation (Dresselhaus et al., 2010; Ferrari et al., 2006). It is seen here that the I_D/I_G decreases monotonically when the electrochemical exfoliation was carried out with SAILs, suggesting less structural damage (defects) when creating graphene compared to those using SDS or SDBS surfactant. Looking to the paper electrical properties, cellulose paper containing graphene with lowest I_D/I_G (those stabilized with BMIM-DBS) give the highest electrical conductivity. As the properties of the resulting composite crucially depend to the quality of RGO and the dispersion stability itself, it is evident that the efficiency of the surfactant performance should be correlated with surfactant chemical structure modification.

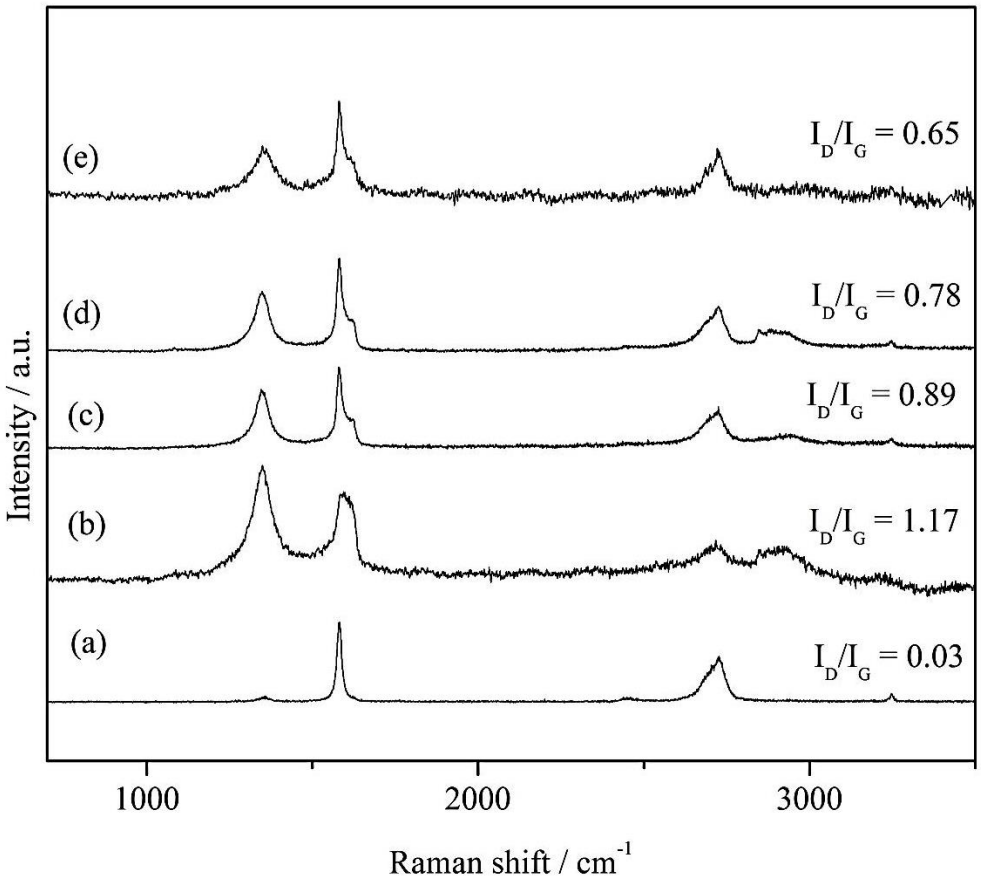

Fig.3. Raman spectra of the graphite (a) and GCPs stabilized surfactant and SAILs (concentration: 0.1 M): (b) SDS, (c) SDBS, (d) BMIM-DS, (e) BMIM-DBS.

3.3 FESEM observation

The micromorphologies of the nanofibrillated kenaf cellulose and GCPs are shown in Fig. 4. Scanning electron microscopy (SEM) images of nanofibrillated kenaf cellulose showed networks of randomly oriented thin fibrils, as shown in Fig. 4a'. The fibers have tap-like morphology with ~ 25 – 50 nm wide. A clearly dispersed RGO sheets was displayed as flakes or tactoids over the surface of cellulose (Fig. 4b-e). Two different domains can be distinguished: a network of cellulose microfibrils and incorporated RGO distributed among them. The bright regions in the images were attributed to the RGOs on account of their high conductivity that can form conducting paths

through and/or across cellulose fibers to render the obtained GCP electrically conductive (Yu et al., 2007).

In respect to GCPs with SDS and SDBS, higher magnification images (Fig. 4b' and 4c') revealed bulk pieces of aggregates throughout cellulose matrix. Interestingly, GCPs with BMIM-DS and BMIM-DBS demonstrated the presence of a nanodispersion of individual RGO flakes suggesting increased exfoliation and dispersion quality over the commercial surfactant. Note that an enlarged view of GCPs with BMIM-DBS offers clearer illustration of RGOs inside the cellulose matrix, in which edges of the upright RGO flakes can be seen (Fig. 4e'), unlike those observed with SDS and SDBS.

The uniform dispersion of RGOs in a polymer matrix is one of the most important requirements for achieving a uniform conductivity throughout the composites (Mohamed et al., 2016; Stankovich et al., 2006; Yu et al., 2007). Here, it can be seen that the higher electrical conductivity enhancement of GCPs with SAILs arises from the well dispersed graphene in the cellulose matrix. It is reasonable to assume that the SAILs are able to mediate a better exfoliation and dispersion of graphene sheets and lessen the tendency of aggregation between the RGO flakes which is beneficial to form 3D-continuous conductive network (Mohamed et al., 2016).

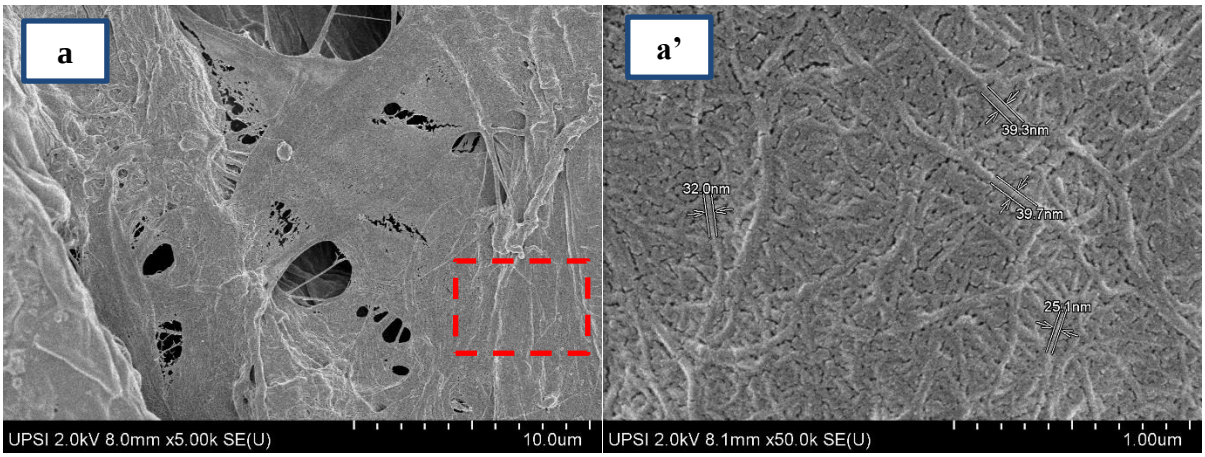

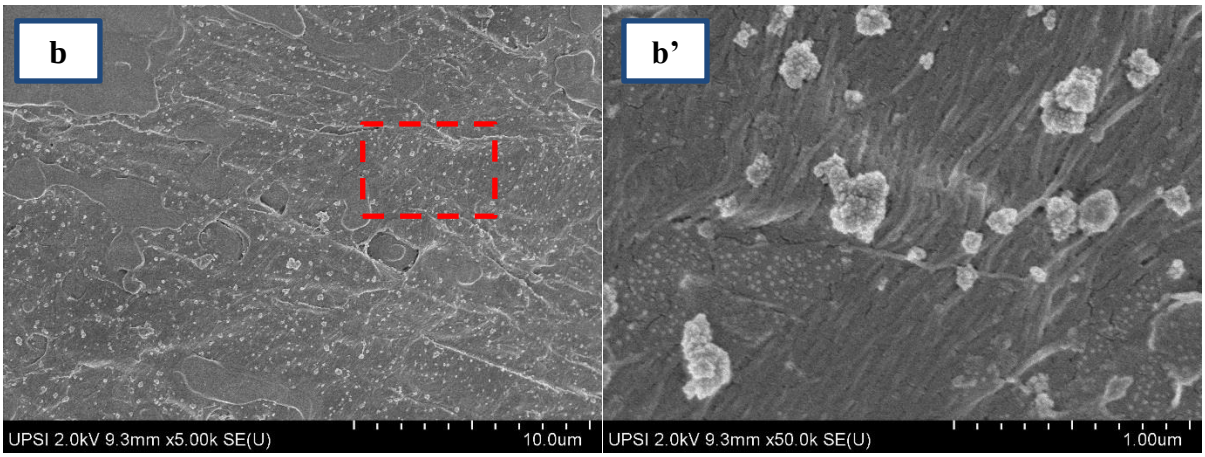
b
UPSI 2.0kV 9.3mm x5.00k SE(U)
10.0um

b'
UPSI 2.0kV 9.3mm x50.0k SE(U)
1.00um

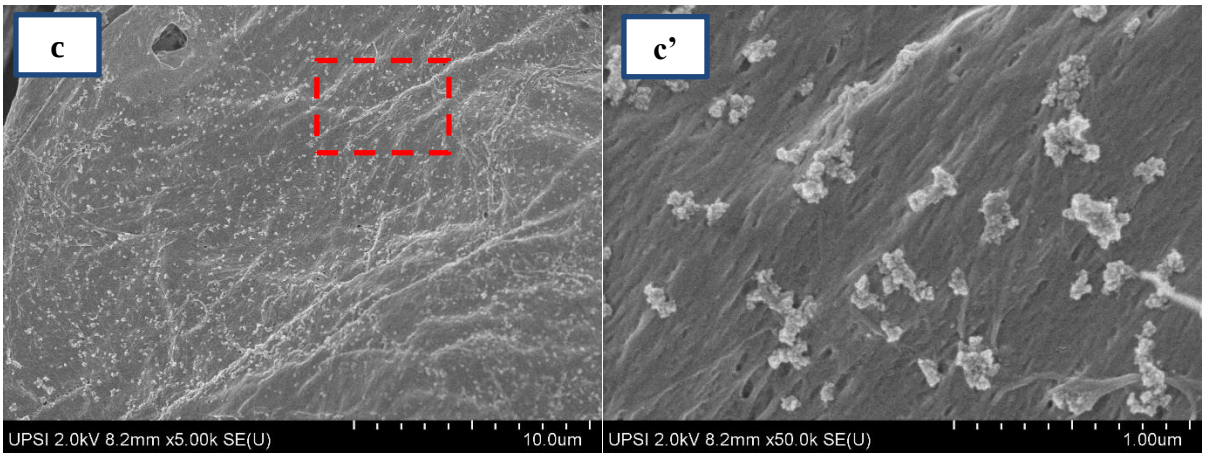
c
UPSI 2.0kV 8.2mm x5.00k SE(U)
10.0um

c'
UPSI 2.0kV 8.2mm x50.0k SE(U)
1.00um

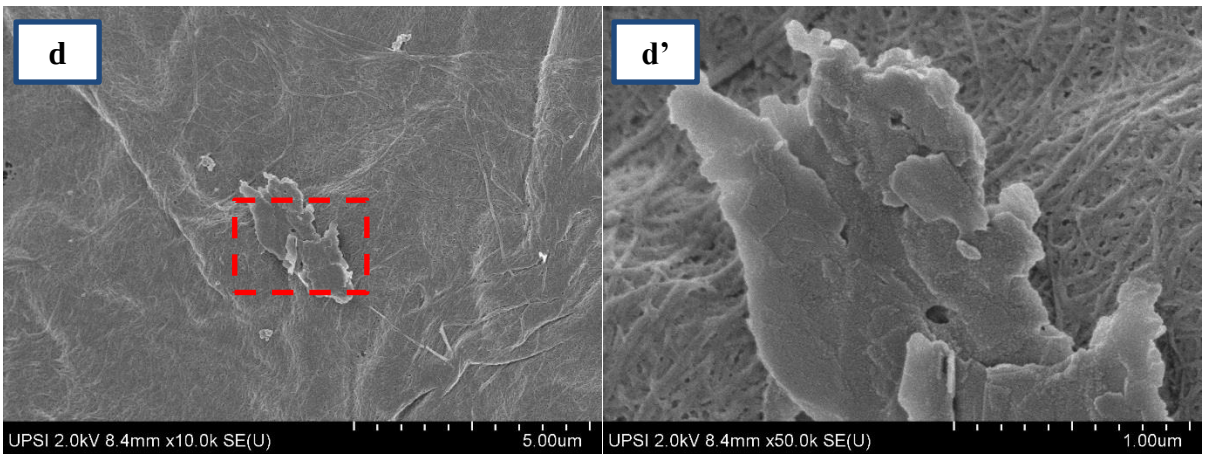
d
UPSI 2.0kV 8.4mm x10.0k SE(U)
5.00um

d'
UPSI 2.0kV 8.4mm x50.0k SE(U)
1.00um

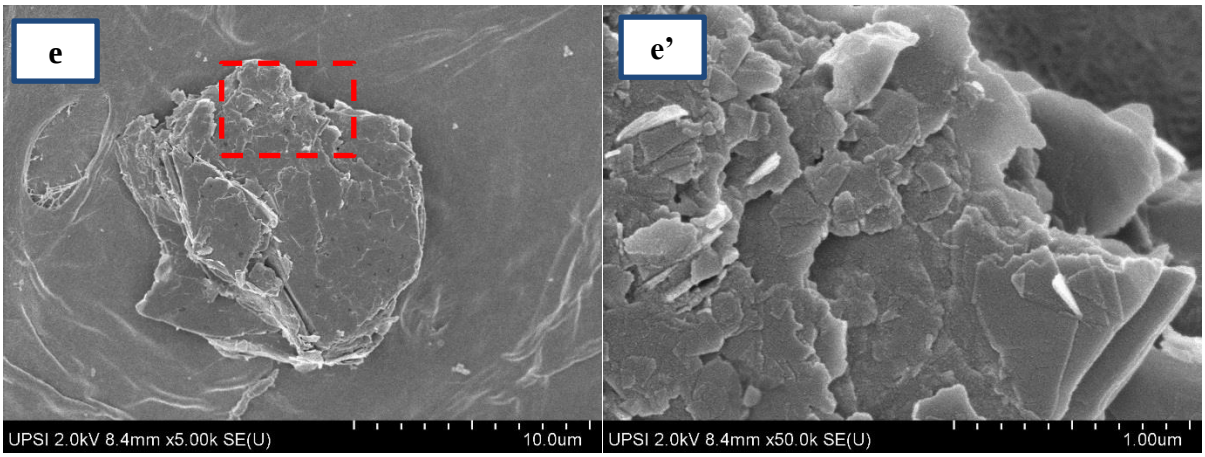

Fig. 4. FESEM images of nanofibrillated kenaf cellulose (a and a'), GCP: with SDS (b and b'), with SDBS (c and c'), with BMIM-DS (d and d') and with BMIM-DBS (e and e'). The area for higher magnification imaging are marked in red square.

3.4 HRTEM

Further morphological characterization was carried out by imaging ultrathin sections of the GCP stabilized with 0.1 M BMIM-DBS under high resolution transmission electron microscopy (HRTEM). In general, TEM is frequently used to image nanosize materials to atomic scale resolution where a transmitted electron beam passes through the ultra-thin sample (Singh et al., 2011). TEM observations at low magnification (Fig. 5a) provide the overall dispersion imaging of RGO in cellulose. It can be seen from Fig. 5b that the spaces between adjacent cellulose fibers are filled with the graphene sheets (Cataldi et al., 2015). It is therefore evident that the RGOs are finely dispersed throughout the cellulose matrix as has been previously revealed by FESEM observations. The enlarged view (Fig. 5c) shows dark lines on the edge of the RGO which indicate the existence of multilayer of graphene in the cellulose matrix (Kang et al., 2012). The reason for good dispersion is probably attributed to the enhanced interfacial interaction between RGO and cellulose

due to the presence of SAILs (Bari et al., 2014; Liu et al., 2008). The possible mechanism behind this unique interaction will be discussed in the following section.

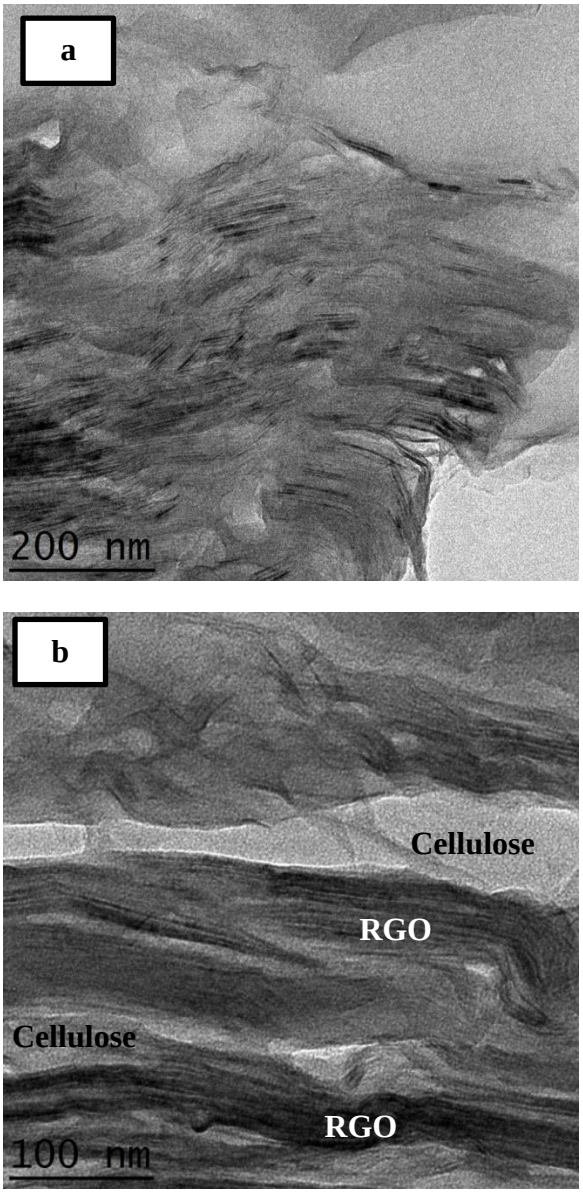

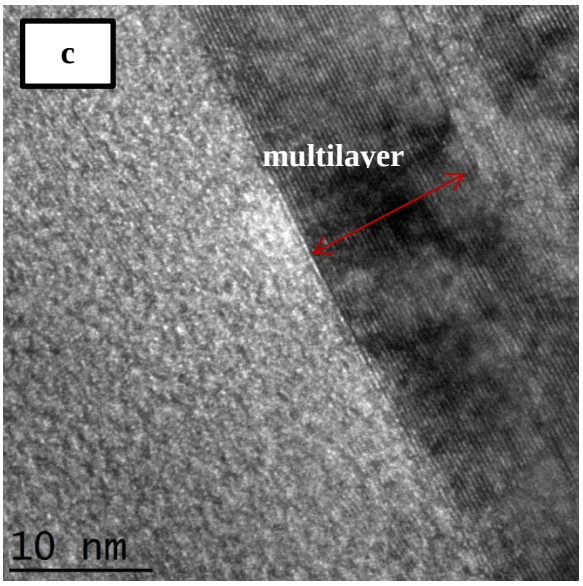

Fig. 5. TEM images of the GCP stabilized BMIM-DBS: (a) typical morpologies at low magnification (b) higher magnification. Grey areas are cellulose fibers. Note that many RGO sheets are embedded throughout cellulose matrix (c) edge view of RGO sheets dispersed in cellulose matrix.

3.5 Studying graphene dispersion stability: zeta potential measurement

As shown above the quality of graphene dispersions can be assessed by microscopy. The important question is which surfactant properties control dispersion quality? Adsorption of ionic surfactants onto graphene imparts an effective charge onto the coated graphene. It is known that the mechanism for the stabilization of graphene dispersions by ionic surfactants is electrostatic repulsion between graphene surfaces owing to adsorbed surfactant molecules. Electrostatic repulsion is generally quantified by the electric potential in the vicinity of the surface of the coated graphene sheets, which is known as the zeta (ζ)-potential (Hunter, 2013). A surfactant-coated graphene is typically surrounded by a tightly bound layer of adsorbed surfactant ions, which, in turn, is surrounded by a more diffuse zone of mobile counterions (Lotya et al., 2009; Sun et al.,

2008). The zeta potential is the potential just beyond the layer of bound surfactant ions, which is at the hydrodynamic slip plane. Graphene coated with charged molecules will display ζ-potentials with a sign reflecting the charge of the adsorbed molecules. Therefore, graphene coated with anionic surfactant should give a negative ζ-potential value.

In general, the dividing line between stable and unstable suspensions is taken as +30 or -30 mV with particles having zeta potentials outside these limits are normally considered stable (Hunter, 2013; Rosen & Kunjappu, 2004). Thus, to achieve stable graphene-coated surfactant dispersions, the ζ-potential should be maximized so that the sheets will tend to repel each other, and there will be no tendency for the particles to come together. It is therefore worthwhile to consider how to achieve graphene-coated surfactant with very high ζ-potential. The most obvious way is by increasing the effective charge of the coated graphene. This can be done by surfactant structure modification, increasing surfactant concentration, pH and so on (Hunter, 2013; Rosen & Kunjappu, 2004).

It can be seen from Table 2 that for all graphene dispersions, the ζ-potential values are lower than -30 mV, underlining the good stability of graphene-surfactant colloidal dispersions. It can be clearly seen here that BMIM-DBS appears to be the most negatively charged of all dispersants, with the increase of nearly 16 mV compare to the parent, SDBS, giving the most stable system out of the surfactants tested in this study. However, the strategy of changing sodium into immidazolium does not always offer significant colloidal stability improvement (in terms of electrostatic stabilization). Noting that for BMIM-DS, the ζ-potential is subtly lower than SDS surfactant. Although when comparing the electrical properties and FESEM observations, BMIM-DS suggest higher affinity compared to SDS, giving moderately higher electrical conductivity and less agglomerated RGO dispersed in the cellulose. Looking only at the ζ-potential measurements,

all the results here are together too small to explain the ability of the SAILs in enhancing the nanocomposite properties.

3.6 Small-angle Neutron Scattering

The nature of surfactant, concentration, and type of interaction are known to play a crucial role in the dispersion behavior of classical colloids. Learning from CNT-aided surfactant dispersion studies, surfactants showed various self-assembly structures which are responsible for the stabilization of the dispersions (Lin et al., 2016; Vaisman, Wagner, & Marom, 2006; Yurekli, Mitchell, & Krishnamoorti, 2004). Here, in an attempt to understand the different aggregation behavior of surfactants in solution and adsorbed on graphene, and to learn the nature of surfactant – graphene interaction for stabilization, small-angle neutron scattering (SANS) has been employed. SANS is the ideal method to provide information regarding the size, shape of surfactant self-assembly structure over the nanometer range that is complementary with microscopy technique. In general, the scattering intensity *I(Q)* is related to the shape, volume, and contrast of the nanoscale structures present in a sample. The contributions to *I(Q)* for a specified shape and size of particle is described by its form factor, *P(Q)*. A comprehensive introductions to small-angle scattering have been published elsewhere (Feigin & Svergun, 1987; Hollamby, 2013). To provide a comparable study, SANS data were collected for all the RGO-stabilized surfactants dispersion and surfactants solutions at similar surfactant concentration and temperature.

The scattering profiles for the surfactants and SAILs (without RGO) were recorded in dilute aqueous phases and are given in Fig. 6. SANS profiles for the sodium analogue – SDS and SDBS, were indicative of charged micelles (see Fig. 6a), showing an obvious charge repulsion *S(Q)* peak following the Hayter-Penfold model (Hayter & Penfold, 1983); others show scattering

characteristic of spherical micelles (Feigin & Svergun, 1987). The fitted micellar dimensions, R_{sphere} for SDS and SDBS both are ~22 Å (Table 3). It is known that both SDS and SDBS forms spherical micelles (Brown et al., 2012; Paul et al., 2005; Yurekli et al., 2004; Wang et al., 2004). Yurekli and his co-workers reported the formation of spherical micelles with R_{sphere} (18 Å at 0.5 wt%; 17 Å at 1 wt%) for SDS even with different concentrations (Yurekli et al., 2004). Magid et al. (2000) also reported spherical micelles with radius of ~ 23 Å for 0.07 M SDS in D_2O at 40°C. The R_{sphere} differences here can be omitted considering experimental error (± 2 Å) and may be related to the difference surfactant concentration itself, as micelle shape and size are may be affected by surfactant concentrations, salt addition, or temperature (Feigin & Svergun, 1987; Hayter & Penfold, 1983). Earlier studies on SDBS using quasielastic light scattering give evidence of the formation sphero-cylinder micelles with R_{sphere} of 22 Å (Cheng & Gulari, 1982). Recent SANS study also reported the formation of 22 Å spherical micelles of SDBS surfactant at 25°C (Mohamed et al., 2018).

Just like normal surfactants, SAILs also showed the ability to self-assemble in aqueous solutions to form micelle (Brown et al., 2011; Brown et al., 2012). The scattering profiles here are consistent with spherical micelle for BMIM-DS. The curves could be fitted with charged spherical micelles with Hayter-Penfold charge repulsion *S(Q)* giving micellar radius of 25 Å. This behavior is analogous to other quartenary ammonium ILs which showed a maintained shape and size of micelle when substituting sodium for tetraalylammonium cations (Brown et al., 2011). Javadian et al. (Javadian, Nasiri, Heydari, Yousefi, & Shahir, 2014) however reported an increase of ~ 10 Å of the micelle radius (assuming that micelles in spherical form conform the Stokes-Einstein equation) when changing sodium into imidazolium counterion measured using light scattering. Imidazolium-based ionic liquids were previously fitted as spherical micelles (Bowers, Butts,

Martin, Vergara-Gutierrez, & Heenan, 2004). Recent research on imidazolium-based SAILs properties reported multilayer stacks model for BMIM-DS and retained the aggregation shape over various concentration (0.5 – 4.0 wt%) (Brown et al., 2012). Moving to BMIM-DBS, this SDBS analogue surprisingly forms cylindrical micelles with a radii of 19 Å and 140 Å in length. In comparison to BMIM-DS, the micelle shape and size transition is much more pronounced. A sphere-to-cylinder transition was previously reported on copolymer ILs comprised of poly(butadiene) and poly(ethyleneoxide) (He, Li, Simone, & Lodge, 2006). They suggested that the transition is encouraged by the preferred interfacial curvature of spherical micelles, when the IL chemical structure lacks a hydrophilic portion (shorter PEO chain). That idea might be in line with the SANS data reported here, considering the presence of a hydrophobic phenyl ring on BMIM-DBS will make it overall less hydrophilic than BMIM-DS. However, none of the other fitted parameters show any obvious trend down the anion series, making it difficult to draw firm conclusions about relationships between cation structure and aggregation.

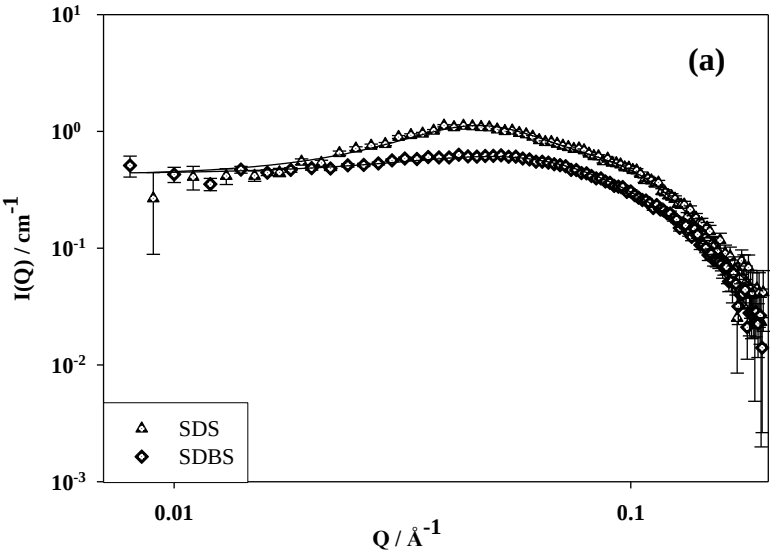

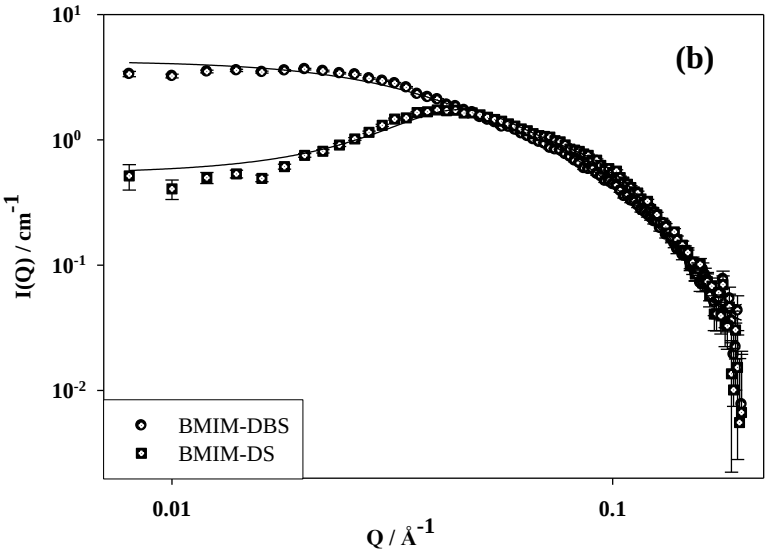
(b)
I(Q) / cm-1
Q / Å-1
BMIM-DBS
BMIM-DS

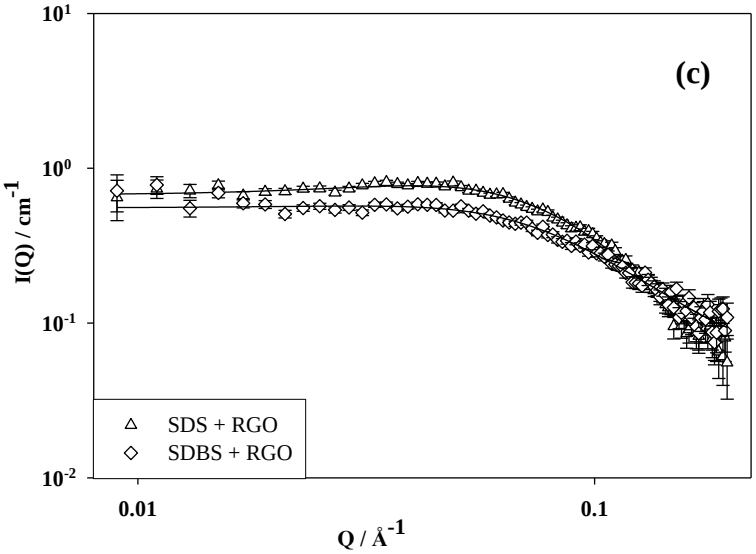
(c)
I(Q) / cm-1
Q / Å-1
SDS + RGO
SDBS + RGO

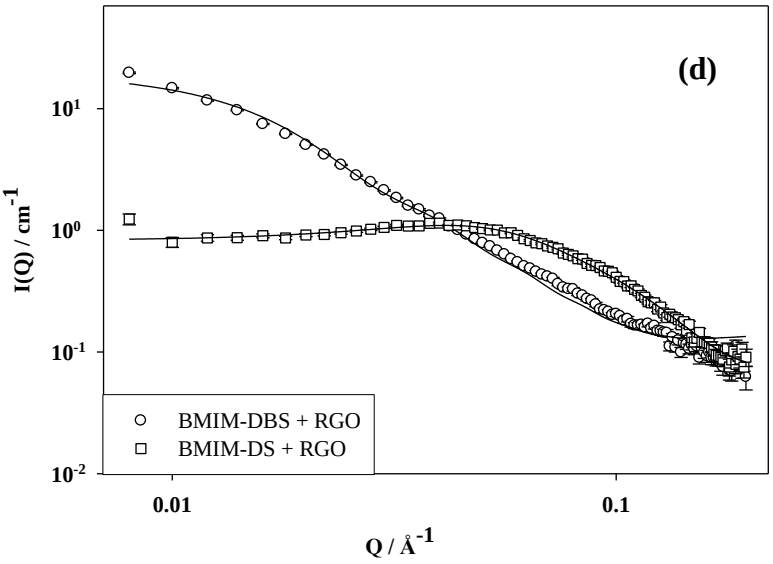

Fig.6 SANS profiles for (a) SDS and SDBS, (b) BMIM-DS and BMIM-DBS solutions and RGO dispersions with (c) SDS and SDBS, (d) BMIM-DS and BMIM-DBS. [Surfactant] = 0.03 M and T = 25 °C. Lines are model fits for charged spherical, ellipsoidal, cylindrical micelles (with Hayter-Penfold S(Q)) or a stacked disk model. Characteristic error bars are shown for the lowest intensity samples.

Again, SANS was used to investigate the aggregate structure in the RGO-stabilized surfactants. SANS profiles for RGO dispersions with SDS, SDBS, BMIM-DS and BMIM-DBS are shown in Fig. 6c and d. The SANS data of an RGO dispersion with SDS were still characteristic of charged spherical aggregates with a Hayter-Penfold *S(Q)*, being reminiscent of the results found for pure SDS. The presence of RGO does not have the effect of increasing the micelle size (considering the experimental error), being R_{sphere} = 24 Å. There is a very small reduction of scattering intensity *I(Q)* throughout the *Q* range compared to pure SDS. This kind of observation has been previously reported with similar surfactants, suggesting the presence of weak interaction between surfactant and graphene surfaces (Mohamed et al., 2018; Yurekli et al., 2004). On the

other hand, there were evolutions in micelle shape and size RGO dispersions with SDBS and BMIM-DS. Both systems have scattering profiles that can be adequately fitted with charged ellipsoidal micelles and a *P(Q)* with polar axis ratio (R_a) and aspect ratio X, multiplied by Hayter-Penfold electrostatic repulsive model. The micellar radii undergo significant changes, giving R_a of 31 Å for SDBS and 40 Å for BMIM-DBS. Consistent with RGO dispersions stabilized by SDS, the scattering profiles exhibit lower *I(Q)*, evident of surfactant adsorption.

Moving to BMIM-DBS, the data reveals Q^{-2} regimes of scattering consistent with a disk-like model (Feigin & Svergun, 1987; Hollamby, 2013), giving a fitted disk radius of 143 Å. In an earlier study of graphene nanoplatelet dispersions with anionic aromatic surfactants, a disk type transition was also found for surfactants with highest dispersion efficiency (highest electrical conductivity enhancement) (Mohamed et al., 2018). Recalling the electrical properties and microscopic observation, BMIM-DBS offers an increased dispersion quality compared to the rest of the stabilizers. That result is consistent with SANS data obtained here. In that work it was assumed that the surfactant adsorbed and wrapped the graphene surfaces giving an appearance as disk-type aggregated structure (Mohamed et al., 2018). Taking all the results together, it is clear that RGO dispersions are present, further ideas for the mechanism on how the surfactant adsorbs on graphene surfaces, and the possible interaction between surfactant and cellulose will be discussed in the following section.

Table 3

Model fit parameters for SANS data[a]

[a][surf.] = 0.030 M. Charged micelles were fitted with interparticle structure factor *S(Q)* for Hayter-Penfold model.

Sample	**Model**	**R_{sphere} (Å)**	**R_a (Å)**	**R_{disk} (Å)**	**$R_{cylinder}$ (Å)**	**X ± 0.2**	**Length (Å)**
SDS	Sphere	22	-	-	-	-	-
SDBS	Sphere	22	-	-	-	-	-
BMIM-DS	Sphere	25	-	-	-	-	-
BMIM-DBS	Cylinder	-	-	-	19	-	140
SDS + RGO	Sphere	24	-	-	-	-	-
SDBS + RGO	Ellipsoid	-	31	-	-	2	-
BMIM-DS + RGO	Ellipsoid	-	40	-	-	2	-
BMIM-DBS + RGO	Stacked disk	-	-	143	-	-	-

3.7 The role of surfactants, SAILs and cellulose for stable graphene dispersions: proposed mechanism

There are many ideas in the literature about the amphiphilic properties of cellulose and that dispersion/dissolution of cellulose in water/solvents are closely related to this duality (Lindman et al., 2010; Medronho & Lindman, 2015). Despite extensive studies on cellulose dissolution using ionic liquids or common surfactants (Lindman et al., 2010; Medronho & Lindman, 2015; Pinkert et al., 2009), the role of individual ionic species involved in dissolution is yet to be fully understood. Regarding the mechanism of dispersion of cellulose in surfactant and SAILs solutions to be used for exfoliating graphite (see Fig. 1), it is assumed that the surfactant/SAIL headgroups

interact with the hydrophilic part of cellulose through hydrogen bonding to render cellulose dispersion in aqueous phase (Lindman et al., 2010; Medronho & Lindman, 2015). Cho and his group, in their study utilizing imidazolium based ILs, suggested that the major driving force for dissolution is the presence of hydrogen bonds between the cationic part of ILs (imidazolium moiety) and the cellulose hydroxyl (Cho, Gross, & Chu, 2011). The cellulose-SAILs and surfactant combination here acted as an electrolyte for electrochemical exfoliation. This is reasonable considering that, when mixing, the cellulose/surfactant or cellulose/SAILs will behave as a typical electrolyte (Lewis & Robinson, 1970).

Literature strongly emphasize that graphene can be prepared using electrochemical methods and stably dispersed in water for a certain period of time when coated by adsorbed surfactants (Abdelkader, Cooper, Dryfe, & Kinloch, 2015; Alanyalıoğlu et al., 2012). In general, electrochemical exfoliation routes to graphene are based on the intercalation of surfactant ions between the layers of graphite rod electrode due to the flow of electrical current. These ions induce expansion of the interlayer space of graphite and thus facilitate exfoliation (Alanyalıoğlu et al., 2012; Parvez et al., 2014). Taking all the results together, it is clear that BMIM-DBS offer increased dispersion quality as compared to others down the series. To understand the molecular interaction underlying this graphene-compatibility, a mechanism is proposed.

Applying bias voltage (7 V) in the electrolyte leads to oxidation at the grain boundaries and edge sites of graphite (Parvez et al., 2014). This results in the opening up of graphite edge sheets. The BMIM-DBS tails are then adsorbed within the edge sheets and initiate the expansion of graphite layers. As a result, exfoliated black powder of expanded graphite oxide was dispersed in the solution after applying electrical current for 24 h. A subsequent peeling process involving low shear forces (ultrasonication) are thought to separate the graphitic material into multilayer

flakes. The materials produced required reduction for deoxygenation of the oxygen-containing functional groups. Typically reduction of graphite oxide substantially reduces the dispersibility in water. Remarkably however, visual observation showed that the resulting dispersion was stable for over 1 month. In this case, BMIM-DBS played a dual role: as an exfoliant/intercalant and a stabilizer for the reduced graphene oxide in the mixture (Alanyalıoğlu et al., 2012; Guardia et al., 2014).

It is believed that the distinct aggregation behaviour of BMIM-DBS is a consequence of the increased RGO surfaces being occupied by BMIM-DBS, wrapping up RGO sheets for stabilization. A previous study revealed that an anionic tri-chain aromatic surfactant namely TC3Ph3 (AZMI ADD THIS chemical name) showed a similar disk-type aggregation due to a full-coverage of surfactant-wrapping the graphene surfaces (Lin et al., 2016; Mohamed et al., 2018). By analogy to that model, it was surmised that BMIM-DBS occupy the graphene faces as much as possible with the tails in contact with the graphene surfaces, driven by the hydrophobic effect (Matarredona et al., 2003; Mohamed et al., 2016). The presence of phenyl rings in the chemical structure undoubtedly provides graphene-affinity as has been noted in extensive literatures (Lin & Xing, 2008; Matarredona et al., 2003; Mohamed et al., 2016; Tkalya, Ghislandi, de With, & Koning, 2012). There is also a possibility of hydrophobic interaction between the hydrophobic part of cellulose and graphene surface considering that cellulose has amphiphilic properties (Lindman et al., 2010; Medronho & Lindman, 2015; Medronho et al., 2012). Indeed, the adsorbed BMIM-DBS along with cellulose shields the attractive van der Waals forces between graphene sheets. The most preferential arrangement of head and tails of BMIM-DBS and cellulose is that BMIM-DBS initially adsorbed with the tail lying flat approaching the graphene surfaces to maximize the hydrophobic interactions and begin wrapping graphene until the surface is saturated. The SAIL

headgroups are hydrogen bonding with cellulose hydroxyls while the hydrophobic part is weakly interacting with graphene leading to a more stabilize dispersion.

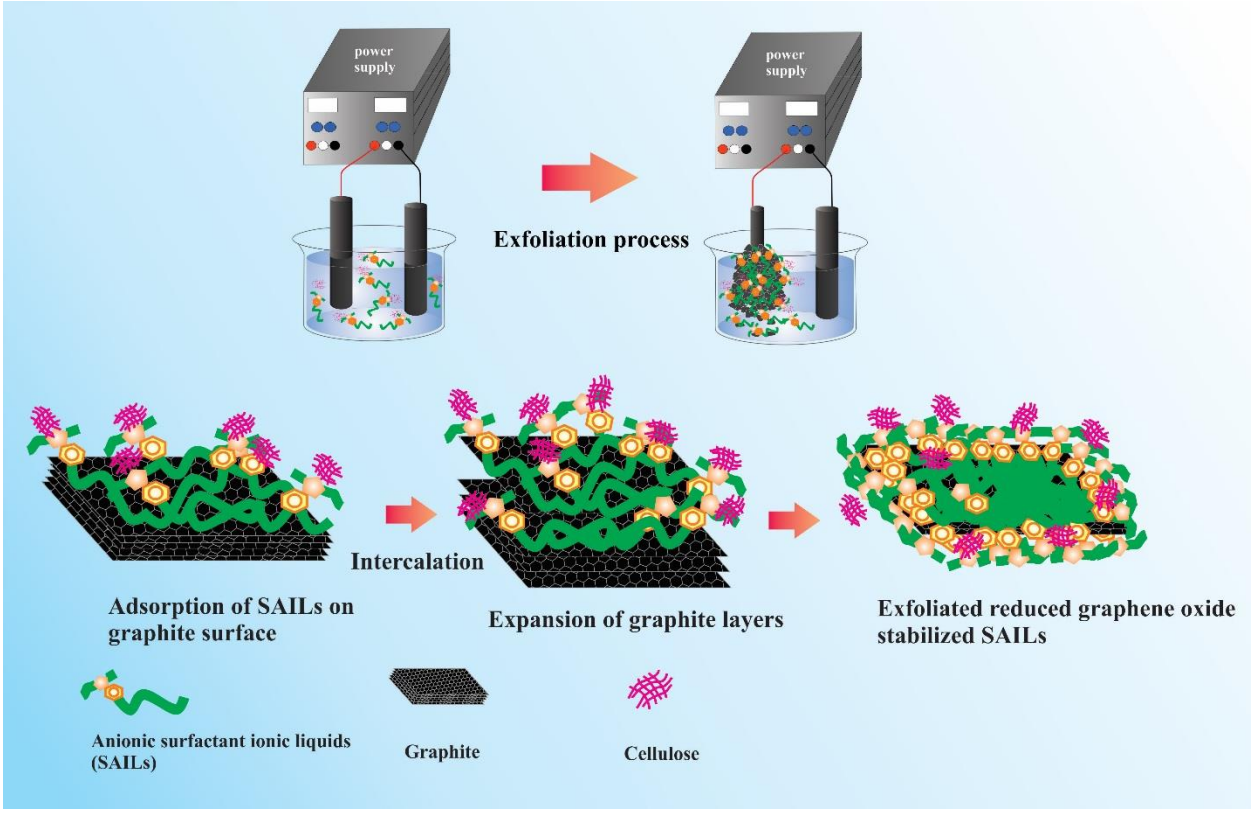

Fig. 7. Schematic illustration the role of anionic surfactant ionic liquids during exfoliation and the interactions with graphene and cellulose particles

4. Conclusions

Graphene and graphene based materials still show great promise in many technological applications, but their large-scale production and processing by simple and cost effective means still constitute significant issues in the path of widespread implementation. Here, this study used a straightforward method for the preparation of ready-to-use material that is based on electrochemical exfoliation of graphite in a mixture of anionic surfactant ionic liquids and cellulose

as the electrolyte. The advantages of this approach over existing methods to produce similar nanocomposite materials are: lower environmental hazards (the medium is water), economically efficient starting materials of ionic liquids, and simple instrumental setup (Parvez et al., 2014; Suriani et al., 2016; Suriani et al., 2015).

Optical microscopy and Raman spectroscopy shows the uniform dispersion of reduced graphene matrix on nanofibrillated kenaf cellulose. Zeta potential measurements reveal increased dispersion stability for BMIM-DBS but firm conclusions on the relationship with counterion type cannot be drawn since BMIM-DS shows a lower zeta potential value. In dilute aqueous phases SANS data indicated transitions in aggregation structure in the presence of graphene for all compounds except SDS. Particularly interesting is how BMIM-DBS induces a cylinder-to-disk transition, all consistent with fully covering surfactant-wrapping of graphene surfaces, deviating from the spherical-to-ellipsoid aggregates seen for the rest compounds (Lin et al., 2016; Matarredona et al., 2003; Mohamed et al., 2018). It does appear that aromatic ring coupled with bulkier counterion type is the best combination, and contributes to the increased graphene compatibility.

The unique combination of surfactant ionic liquids with polymer as a greener exfoliating medium may pave the way to development of novel nanocomposite processing routes. Furthermore, these economical and efficient SAILs alone may find applications as both exfoliating agents and dispersants for other layered or two dimensional materials such as metal dichalcogenides and metal-organic frameworks (Mas-Balleste, Gomez-Navarro, Gomez-Herrero, & Zamora, 2011). This graphene conductive cellulose paper produced here may also find applications in electronic devices as flexible supercapacitors, electrodes, or sensors (Hou, Xu, & Li, 2018; Weng et al., 2011).

Acknowledgements

The work funded under grants from Kurita Water and Environment Foundation (Grant Code: 16P003), and the Fundamental Research Grant Scheme (FRGS; Grant code: 2015-0155-101-02). This project was supported by JSPS [KAKENHI, Grant-in-Aid for Young Scientists (A), No. 23685034], KAKENHI, Grant-in-Aid for Scientific Research (B), No. 26289345, Fund for the Promotion of Joint International Research (Fostering Joint International Research) No. 15KK0221, Grant-in-Aid for Challenging Research (Exploratory), No.17K19002] and Leading Research Organizations (RCUK [through EPSRC EP/I018301/1], ANR [13-G8ME-0003]) under the G8 Research Councils Initiative for Multi-lateral Research Funding— G8-2012. The authors thank the Science and Technology Facilities Council for allocation of beam time, travel and consumables (experiment number RB1710004). This work benefited from the use of the SasView application, originally developed under NSF Award DMR-0520547. SasView also contains code developed with funding from the EU Horizon 2020 programme under the SINE2020 project Grant No 654000.

References

Abdelkader, A. M., Cooper, A. J., Dryfe, R. A. W., & Kinloch, I. A. (2015). How to get between the sheets: a review of recent works on the electrochemical exfoliation of graphene materials from bulk graphite. *Nanoscale, 7*, 6944-6956.

Abdul Khalil, H. P. S., Bhat, A. H., & Ireana Yusra, A. F. (2012). Green composites from sustainable cellulose nanofibrils: A review. *Carbohydrate polymers, 87*, 963-979.

Abdul Khalil, H. P. S., Ireana Yusra, A. F., Bhat, A. H., & Jawaid, M. (2010). Cell wall ultrastructure, anatomy, lignin distribution, and chemical composition of Malaysian cultivated kenaf fiber. *Industrial Crops and Products, 31*, 113-121.

Alanyalıoğlu, M., Segura, J. J., Oró-Solè, J., & Casañ-Pastor, N. (2012). The synthesis of graphene sheets with controlled thickness and order using surfactant-assisted electrochemical processes. *Carbon, 50*, 142-152.

Bari, R., Tamas, G., Irin, F., Aquino, A. J. A., Green, M. J., & Quitevis, E. L. (2014). Direct exfoliation of graphene in ionic liquids with aromatic groups. *Colloids and Surfaces A: Physicochemical and Engineering Aspects, 463*, 63-69.

Bowers, J., Butts, C. P., Martin, P. J., Vergara-Gutierrez, M. C., & Heenan, R. K. (2004). Aggregation behavior of aqueous solutions of ionic liquids. *Langmuir, 20*, 2191-2198.

Brown, P., Butts, C., Dyer, R., Eastoe, J., Grillo, I., Guittard, F, Rogers, S., & Heenan, R. (2011). Anionic surfactants and surfactant ionic liquids with quaternary ammonium counterions. *Langmuir, 27*, 4563-4571.

Brown, P., Butts, C. P., Eastoe, J., Fermin, D., Grillo, I., Lee, H.-C., Parker, D., Plana, D., & Richardson, R. M. (2012). Anionic surfactant ionic liquids with 1-butyl-3-methyl-imidazolium cations: characterization and application. *Langmuir, 28*, 2502-2509.

Cataldi, P., Bayer, I. S., Bonaccorso, F., Pellegrini, V., Athanassiou, A., & Cingolani, R. (2015). Foldable conductive cellulose fiber networks modified by graphene nanoplatelet-bio-based composites. *Advanced Electronic Materials, 1*, 1500224 (1-8).

Cheng, D. C. H., & Gulari, E. (1982). Micellization and intermicellar interactions in aqueous sodium dodecyl benzene sulfonate solutions. *Journal of Colloid and Interface Science, 90*, 410-423.

Chiappe, C., & Pieraccini, D. (2005). Ionic liquids: solvent properties and organic reactivity. *Journal of Physical Organic Chemistry, 18*, 275-297.

Cho, H. M., Gross, A. S., & Chu, J.-W. (2011). Dissecting force interactions in cellulose deconstruction reveals the required solvent versatility for overcoming biomass recalcitrance. *Journal of the American Chemical Society, 133*, 14033-14041.

Dresselhaus, M. S., Jorio, A., Hofmann, M., Dresselhaus, G., & Saito, R. (2010). Perspectives on carbon nanotubes and graphene Raman spectroscopy. *Nano Letters, 10*, 751-758.

Earle, M. J., & Seddon, K. R. (2000). Ionic liquids. Green solvents for the future. *Pure and Applied Chemistry, 72*, 1391-1398.

Feigin, L. A., & Svergun, D. I. (1987). *Structure analysis by small-angle X-ray and neutron scattering*. (1st ed). New York: Springer, (Chapter 1).

Feng, Y., Zhang, X., Shen, Y., Yoshino, K., & Feng, W. (2012). A mechanically strong, flexible and conductive film based on bacterial cellulose/graphene nanocomposite. *Carbohydrate polymers, 87*, 644-649.

Ferrari, A. C., Meyer, J. C., Scardaci, V., Casiraghi, C., Lazzeri, M., Mauri, F., Piscanec, C., Jiang, D., Novoselov, K. S., Roth, S., & Geim, A. K. (2006). Raman spectrum of graphene and graphene Layers. *Physical Review Letters, 97*, 187401.

Guardia, L., Paredes, J. I., Rozada, R., Villar-Rodil, S., Martínez-Alonso, A., & Tascón, J. M. D. (2014). Production of aqueous dispersions of inorganic graphene analogues by exfoliation and stabilization with non-ionic surfactants. *RSC Advances, 4*, 14115-14127.

Hayter, J. B., & Penfold, J. (1983). Determination of micelle structure and charge by neutron small-angle scattering. *Colloid & Polymer Science, 261*, 1022-1030.

He, Y., Li, Z., Simone, P., & Lodge, T. P. (2006). Self-assembly of block copolymer micelles in an ionic liquid. *Journal of the American Chemical Society, 128,* 2745-2750.

Hernandez, Y., Lotya, M., Rickard, D., Bergin, S. D., & Coleman, J. N. (2009). Measurement of multicomponent solubility parameters for graphene facilitates solvent discovery. *Langmuir, 26,* 3208-3213.

Hollamby, M. J. (2013). Practical applications of small-angle neutron scattering. *Physical Chemistry Chemical Physics, 15,* 10566-10579.

Hou, M., Xu, M., & Li, B. (2018). Enhanced electrical conductivity of cellulose nanofiber/graphene composite paper with a sandwich structure. *ACS Sustainable Chemistry & Engineering, 6,* 2983-2990.

Hunter, R. J. (1981). *Zeta potential in colloid science: principles and applications*. (1st ed.). London: Academic Press, (Chapter 2).

Javadian, S., Nasiri, F., Heydari, A., Yousefi, A., & Shahir, A. A. (2014). Modifying effect of imidazolium-based ionic liquids on surface activity and self-assembled nanostructures of sodium dodecyl sulfate. *The Journal of Physical Chemistry B, 118,* 4140-4150.

Kakaei, K., & Hasanpour, K. (2014). Synthesis of graphene oxide nanosheets by electrochemical exfoliation of graphite in cetyltrimethylammonium bromide and its application for oxygen reduction. *Journal of Materials Chemistry A, 2,* 15428-15436.

Kang, Y.-R., Li, Y.-L., Hou, F., Wen, Y.-Y., & Su, D. (2012). Fabrication of electric papers of graphene nanosheet shelled cellulose fibres by dispersion and infiltration as flexible electrodes for energy storage. *Nanoscale, 4,* 3248-3253.

Kiziltas, E. E., Kiziltas, A., Rhodes, K., Emanetoglu, N. W., Blumentritt, M., & Gardner, D. J. (2016). Electrically conductive nano graphite-filled bacterial cellulose composites. *Carbohydrate polymers, 136*, 1144-1151.

Lewis, K. E., & Robinson, C. P. (1970). The interaction of sodium dodecyl sulfate with methyl cellulose and polyvinyl alcohol. *Journal of Colloid and Interface Science, 32*, 539-546.

Lin, D., & Xing, B. (2008). Adsorption of phenolic compounds by carbon nanotubes: role of aromaticity and substitution of hydroxyl groups. *Environmental Science & Technology, 42*, 7254-7259.

Lin, S., Shih, C.-J., Sresht, V., Rajan, A. G., Strano, M. S., & Blankschtein, D. (2016). Understanding the colloidal dispersion stability of 1D and 2D materials: perspectives from molecular simulations and theoretical modeling. *Advances in Colloid and Interface Science, 244*, 36-53.

Lindman, B., Karlström, G., & Stigsson, L. (2010). On the mechanism of dissolution of cellulose. *Journal of Molecular Liquids, 156*, 76-81.

Liu, N., Luo, F., Wu, H., Liu, Y., Zhang, C., & Chen, J. (2008). One–step ionic–liquid–assisted electrochemical synthesis of ionic–functionalized graphene sheets directly from graphite. *Advanced Functional Materials, 18*, 1518-1525.

Lotya, M., Hernandez, Y., King, P. J., Smith, R. J., Nicolosi, V., Karlsson, L. S., Blighe, F. M., De, S., Wang, Z., McGovern, I. T., Duesberg, G. S., & Coleman, J. N. (2009). Liquid phase production of graphene by exfoliation of graphite in surfactant/water solutions. *Journal of the American Chemical Society, 131*, 3611-3620.

Magid, L. J., Li, Z., & Butler, P. D. (2000). Flexibility of elongated sodium dodecyl sulfate micelles in aqueous sodium chloride: a small-angle neutron scattering study. *Langmuir, 16*, 10028-10036.

Mas-Balleste, R., Gomez-Navarro, C., Gomez-Herrero, J., & Zamora, F. (2011). 2D materials: to graphene and beyond. *Nanoscale, 3*, 20-30.

Matarredona, O., Rhoads, H., Li, Z., Harwell, J. H., Balzano, L., & Resasco, D. E. (2003). Dispersion of single-walled carbon nanotubes in aqueous solutions of the anionic surfactant NaDDBS. *The Journal of Physical Chemistry B, 107*, 13357-13367.

Medronho, B., & Lindman, B. (2014). Competing forces during cellulose dissolution: from solvents to mechanisms. *Current Opinion in Colloid & Interface Science, 19*, 32-40.

Medronho, B., & Lindman, B. (2015). Brief overview on cellulose dissolution/regeneration interactions and mechanisms. *Advances in colloid and interface science, 222*, 502-508.

Medronho, B., Romano, A., Miguel, M. G., Stigsson, L., & Lindman, B. (2012). Rationalizing cellulose (in) solubility: reviewing basic physicochemical aspects and role of hydrophobic interactions. *Cellulose, 19*, 581-587.

Mohamed, A., Ardyani, T., Abu Bakar, S., Sagisaka, M., Umetsu, Y., Hamon, J. J., Rahim, B. A., Esa, S. R., Abdul Khalil, H. P. S., Mamat, M. H., King, S., & Eastoe, J. (2018). Rational design of aromatic surfactants for graphene/natural rubber latex nanocomposites with enhanced electrical conductivity. *Journal of Colloid and Interface Science, 516*, 34-47.

Mohamed, A., Ardyani, T., Bakar, S. A., Brown, P., Hollamby, M., Sagisaka, M., & Eastoe, J. (2016). Graphene-philic surfactants for nanocomposites in latex technology. *Advances in Colloid and Interface Science, 230*, 54-69.

Nuvoli, D., Valentini, L., Alzari, V., Scognamillo, S., Bon, S. B., Piccinini, M., Illescas, J., & Mariani, A. (2011). High concentration few-layer graphene sheets obtained by liquid phase exfoliation of graphite in ionic liquid. *Journal of Materials Chemistry, 21*, 3428-3431.

Parvez, K., Wu, Z.-S., Li, R., Liu, X., Graf, R., Feng, X., & Müllen, K. (2014). Exfoliation of graphite into graphene in aqueous solutions of inorganic salts. *Journal of the American Chemical Society, 136*, 6083-6091.

Paul, A., Griffiths, P. C., Pettersson, E., Stilbs, P., Bales, B. L., Zana, R., & Heenan, R. K. (2005). Nuclear magnetic resonance and small-angle neutron scattering studies of anionic surfactants with macrocounterions: tetramethylammonium dodecyl sulfate. *The Journal of Physical Chemistry B, 109*, 15775-15779.

Pinkert, A., Marsh, K. N., Pang, S., & Staiger, M. P. (2009). Ionic liquids and their interaction with cellulose. *Chemical Reviews, 109*, 6712-6728.

Rosen, M. J. (2004). *Surfactants and interfacial phenomena*. (3rd ed.) New Jersey: John Wiley & Sons, (Chapter 9).

Roy, D., Semsarilar, M., Guthrie, J. T., & Perrier, S. (2009). Cellulose modification by polymer grafting: a review. *Chemical Society Reviews*, *38*, 2046-2064.

Singh, V., Joung, D., Zhai, L., Das, S., Khondaker, S. I., & Seal, S. (2011). Graphene based materials: Past, present and future. *Progress in Materials Science, 56*, 1178-1271.

Stankovich, S., Dikin, D. A., Dommett, G. H. B., Kohlhaas, K. M., Zimney, E. J., Stach, E. A., Piner, R. D., Nguyen, SB. T., & Ruoff, R. S. (2006). Graphene-based composite materials. *Nature, 442*, 282-286.

Sun, Z., Nicolosi, V., Rickard, D., Bergin, S. D., Aherne, D., & Coleman, J. N. (2008). Quantitative evaluation of surfactant-stabilized single-walled carbon nanotubes: dispersion quality and its correlation with zeta potential. *The Journal of Physical Chemistry C, 112*, 10692-10699.

Suriani, A. B., Nurhafizah, M. D., Mohamed, A., Masrom, A. K., Sahajwalla, V., & Joshi, R. K. (2016). Highly conductive electrodes of graphene oxide/natural rubber latex-based electrodes by using a hyper-branched surfactant. *Materials & Design, 99*, 174-181.

Suriani, A. B., Nurhafizah, M. D., Mohamed, A., Zainol, I., & Masrom, A. K. (2015). A facile one-step method for graphene oxide/natural rubber latex nanocomposite production for supercapacitor applications. *Materials Letters, 161*, 665-668.

Tkalya, E. E., Ghislandi, M., de With, G., & Koning, C. E. (2012). The use of surfactants for dispersing carbon nanotubes and graphene to make conductive nanocomposites. *Current Opinion in Colloid & Interface Science, 17*, 225-232.

Vaisman, L., Wagner, H. D., & Marom, G. (2006). The role of surfactants in dispersion of carbon nanotubes. *Advances in Colloid and Interface Science, 128-130*, 37-46.

Wang, S., Yi, M., & Shen, Z. (2016). The effect of surfactants and their concentration on the liquid exfoliation of graphene. *RSC Advances, 6*, 56705-56710.

Weng, Z., Su, Y., Wang, D.-W., Li, F., Du, J., & Cheng, H.-M. (2011). Graphene-cellulose paper flexible supercapacitors. *Advanced Energy Materials, 1*, 917-922.

Whitener Jr, K. E., & Sheehan, P. E. (2014). Graphene synthesis. *Diamond and Related Materials, 46*, 25-34.

Ye, W., Li, X., Zhu, H., Wang, X., Wang, S., Wang, H., & Sun, R. (2016). Green fabrication of cellulose/graphene composite in ionic liquid and its electrochemical and photothermal properties. *Chemical Engineering Journal, 299*, 45-55.

Yoon, S. H., Jin, H.-J., Kook, M.-C., & Pyun, Y. R. (2006). Electrically conductive bacterial cellulose by incorporation of carbon nanotubes. *Biomacromolecules, 7*, 1280-1284.

Yu, J., Lu, K., Sourty, E., Grossiord, N., Koning, C. E., & Loos, J. (2007). Characterization of conductive multiwall carbon nanotube/polystyrene composites prepared by latex technology. *Carbon, 45*, 2897-2903.

Yurekli, K., Mitchell, C. A., & Krishnamoorti, R. (2004). Small-angle neutron scattering from surfactant-assisted aqueous dispersions of carbon nanotubes. *Journal of the American Chemical Society, 126*, 9902-9903.

Zhang, J., Zhang, J., Lin, L., Chen, T., Zhang, J., Liu, S., Li, Z., & Ouyang, P. (2009). Dissolution of microcrystalline cellulose in phosphoric acid-molecular changes and kinetics. *Molecules, 14*, 5027-5041.

Zhang, X., Liu, X., Zheng, W., & Zhu, J. (2012). Regenerated cellulose/graphene nanocomposite films prepared in DMAC/LiCl solution. *Carbohydrate polymers, 88*, 26-30.

Zhou, J., & Zhang, L. (2000). Solubility of cellulose in NaOH/urea aqueous solution. *Polymer Journal, 32*, 866-870.

Zhou, W., Islam, M. F., Wang, H., Ho, D. L., Yodh, A. G., Winey, K. I., & Fischer, J. E. (2004). Small angle neutron scattering from single-wall carbon nanotube suspensions: evidence for isolated rigid rods and rod networks. *Chemical Physics Letters, 384*, 185-189.

Zhu, S., Wu, Y., Chen, Q., Yu, Z., Wang, C., Jin, S., Ding, Y., & Wu, G. (2006). Dissolution of cellulose with ionic liquids and its application: a mini-review. *Green Chemistry, 8*, 325-327.